Organic Electronics 27 (2015) 240–246

Contents lists available at ScienceDirect

Organic Electronics

journal homepage: www.elsevier.com/locate/orgel

Interface effect in pentacene field-effect transistors from high energy proton beam irradiation

Tae-Young Kim [a], Jingon Jang [a], Kyungjune Cho [a], Younggul Song [a], Woanseo Park [a], Jinsu Park [a], Jae-Keun Kim [a], Woong-Ki Hong [b,**], Takhee Lee [a,*]

[a] Department of Physics and Astronomy, and Institute of Applied Physics, Seoul National University, Seoul 08826, South Korea
[b] Jeonju Center, Korea Basic Science Institute, Jeonju, Jeollabuk-do 54907, South Korea

ARTICLE INFO

Article history:
Received 12 August 2015
Received in revised form
19 September 2015
Accepted 28 September 2015

Keywords::
Organic field-effect transistor
Proton beam irradiation
Pentacene
Electronic transport properties
Interface trapped charges

ABSTRACT

We report the effect of irradiation using 10 MeV high energy proton beams on pentacene organic field-effect transistors (OFETs). The electrical characteristics of the pentacene OFETs were measured before and after proton beam irradiation with fluence (dose) conditions of 10^{12}, 10^{13}, and 10^{14} cm^{-2}. After proton beam irradiation with fluences of 10^{12} or 10^{13} cm^{-2}, the threshold voltage of the OFET devices shifted to the positive gate voltage direction with an increase in the current level and mobility. In contrast, for a high proton beam fluence condition of 10^{14} cm^{-2}, the threshold voltage shifted to the negative gate voltage direction with a decrease in the current level and mobility. It is evident from the electrical characteristics of the pentacene OFETs treated with a self-assembled monolayer that these experimental observations can be attributed to the trapped charges in the dielectric layer and pentacene/SiO_2 interface. Our study will enhance the understanding of the influence of high energy particles on organic field-effect transistors.

© 2015 Elsevier B.V. All rights reserved.

1. Introduction

Organic electronic devices have been widely explored due to potential advantages including a variety of material choices, an easy fabrication process, low-cost mass production, flexibility, and printability [1–5]. Especially, organic field-effect transistors (OFETs) are important elements in contemporary electronics due to their wide range of potential applications such as identification tags, electronic bar codes, and active matrix elements for displays [6–9]. So, many research efforts have been devoted to the characterization and understanding of OFETs made from various organic materials, as well as the enhancement of the electrical performance of these devices [10–13]. The electrical characteristics of OFETs such as current levels, on/off ratio, mobility, and operational turn-on voltage (or threshold voltage) play critical roles in understanding the device operation and developing optimized devices, especially with respect to the charge injection and transport through the interface.

In particular, to fully tailor the fascinating electrical properties of OFETs into next generation electronics, we need to control the threshold voltage and mobility. The threshold voltage and mobility values of OFETs are highly affected by the semiconductor–dielectric interface [14–16]. In that context, there have been many studies about modification of the semiconductor–dielectric interface in various ways. For example, Kang et al. showed the enhanced device performance of rubrene OFETs by using graphene and hexagonal boron nitride as the electrodes and gate dielectric layers recently [17]. Due to charge-trap free clean hexagonal boron nitride and graphene interface, field effect mobility increased and hysteresis was suppressed. Furthermore, there have been studies on improving the electrical properties of OFETs through modifying inorganic surfaces or interfaces using functional molecules, including self-assembled monolayers (SAMs) [18–20]. These inserted SAMs could reduce the density of interface trap states and improve the morphology of the active pentacene layers. Others have modified the operation properties of OFETs by irradiation with ultraviolet (UV) light or gamma rays [21,22]. UV light irradiation resulted in electron trapping at the pentacene/dielectric interface and the pentacene OFET's electrical characteristics changed due to the slow release of trapped electrons. On the other hand, high energy gamma ray irradiation induced positive hole trapping in the

* Corresponding author.
** Corresponding author.
E-mail addresses: wkh27@kbsi.re.kr (W.-K. Hong), tlee@snu.ac.kr (T. Lee).

http://dx.doi.org/10.1016/j.orgel.2015.09.029
1566-1199/© 2015 Elsevier B.V. All rights reserved.

SiO_2 layer of pentacene OFETs.

But, as far as we know, there have been no studies on high energy proton beam irradiation effects on the pentacene/SiO_2 interface of pentacene OFETs to control the threshold voltage or mobility. Considering several previous studies about tuning the electrical characteristics of pentacene OFETs by irradiating the high energy proton beams to inorganic FETs [23–25], we could expect tuning the electrical characteristics by proton beam irradiation. It is well-known that when high energy beams of charged particles are incident on FET devices, beams induce the trapped charges in the dielectric layer and the semiconductor/dielectric interface. And these trapped charges affect carriers of the active material of devices [26,27]. As a result of these trapped charges, the electrical properties of devices can be tailored. Besides, high energy proton beam irradiation experiments on pentacene OFETs could be a good opportunity to see the application of pentacene OFETs in aerospace radiation environment [28].

In this study, we investigated the electrical characteristics of pentacene OFET devices on SiO_2/p++Si substrates through 10 MeV high energy proton beam irradiation. We systematically characterized the electrical properties of pentacene OFET devices before and after proton beam irradiation with different beam irradiation time conditions. We also studied the effect of proton beam irradiation on pentacene OFETs when the dielectric surface was coated with a passivating octadecyltrichlorosilane (OTS) SAM. The proton beam irradiation effects on the pentacene OFETs were analyzed based on the interplay between the proton beam irradiation-induced trapped charges inside the SiO_2 dielectric layer and at the pentacene/SiO_2 interface.

2. Experimental

2.1. Device fabrication

For the pentacene OFET device fabrication, a SiO_2 (270 nm-thick)/p++Si substrate was prepared and cleaned by dipping in an ultrasonic bath of acetone, isopropyl alcohol, and de-ionized water for 5 min at each step. The source and drain electrodes were prepared by depositing Au (30 nm)/Ti (5 nm) layers using an electron beam evaporator with a deposition rate of 0.5 Å/s at a pressure of ~10^{-7} Torr. The active channel was prepared by depositing a 60 nm-thick pentacene film using a thermal evaporator with a deposition rate of 0.5 Å/s at a pressure of ~10^{-6} Torr. For the molecular treatment on the pentacene OFETs, we deposited an octadecyltrichlorosilane (OTS) self-assembled monolayer (SAM) on the SiO_2 layer surface by immersing the sample in a silane solution (0.1 wt. %) in anhydrous toluene for ~12 h under a N_2 atmosphere. The chemically treated samples were cleaned in toluene for 20 min and dried by blowing N_2 gas.

2.2. Proton beam irradiation

The proton beam irradiation experiments were performed using an MC-50 cyclotron at the Korea Institute of Radiological and Medical Science. The proton beam had an energy of 10 MeV, an average beam current of 10 nA, and a beam uniformity of approximately 90%.

2.3. Characterization of materials

X-Ray diffraction (XRD) measurements were taken using a D8-ADVANCE (Bruker) with Cu Kα radiation at the Center for Materials Analysis at Seoul National University. AFM measurements were taken using an NX 10 AFM system (Park Systems).

2.4. Measurement of electrical characteristics

We measured the electrical characteristics of pentacene OFET devices using a semiconductor characterization system (Keithley 4200-SCS) and a probe station (JANIS ST-500) at room temperature in a vacuum (~10^{-4} Torr).

3. Results and discussion

Fig. 1a shows a schematic illustration of proton beam irradiation on a pentacene OFET device. The fabrication process of the pentacene OFET devices is as follows. First, a Si wafer with a 270 nm-thick SiO_2 dielectric layer was cleaned by a standard solvent cleaning process. Au (30 nm)/Ti (5 nm) layers were then deposited as the source and drain electrodes on the Si wafer through a patterned shadow mask using an electron beam evaporator. Next, we deposited a 60 nm-thick pentacene active layer using a thermal evaporator. More details of the device fabrication process are explained in the Experimental Section and in the Supplementary Data (Fig. S1). Fig. 1b shows optical microscope images of the fabricated pentacene OFET devices. The right one is the image of entire device and the left one is enlarged one. The channel length and width of the OFETs are 100 and 300 μm, respectively.

Following the electrical measurements of the pentacene OFET devices, a 10 MeV proton beam was irradiated onto the top-surface of pentacene OFET devices using a proton beam facility (MC-50 cyclotron) at the Korea Institute of Radiological and Medical Sciences (see the schematic image of Fig. 1a). Different proton beam irradiation times of 20, 200, and 2000 s were used, which correspond to a total fluence (or dose; the number of irradiated particles per unit area) values Φ of ~10^{12}, 10^{13}, and 10^{14} cm^{-2}, respectively. The electrical characteristics of each device were systematically measured and compared before and after the proton beam irradiation. For statistical analysis, we measured more than five devices for each proton beam irradiation condition.

Fig. 1c–f present the representative electrical characteristics of the pentacene OFET devices before and after the devices were irradiated with proton beams. Fig. 1c shows the output characteristics (source-drain current versus source-drain voltage, I_{DS}–V_{DS}) for a pentacene OFET measured at gate voltages (V_G) varying from 30 to −30 V with a step of 10 V before and after the proton beam irradiation with a fluence of 10^{12} cm^{-2}, corresponding to a beam irradiation time of 20 s Fig. 1d shows the semilogarithmic plot of transfer characteristics (source-drain current versus gate voltage, I_{DS}–V_G) measured for the same device at a fixed source-drain voltage (V_{DS}) of −40 V before and after proton irradiation with a fluence of 10^{12} cm^{-2}. This is also plotted on the linear y-axis in the inset of Fig. 1d. Fig. 1e and f show the output and transfer characteristics, respectively, measured for another pentacene OFET device before and after proton beam irradiation with a higher fluence condition of 10^{14} cm^{-2}, corresponding to a longer irradiation time of 2000 s. Notably, we observed that the pentacene OFET devices under different proton beam irradiation conditions exhibited distinct electrical behaviors. When the devices were irradiated with a fluence of 10^{12} cm^{-2}, we observed that the source-drain current of the device increased (Fig. 1c and d), with the current of ~2.6 μA at $V_{DS} = -30$ V and $V_G = -30$ V before the proton beam irradiation increasing to ~3.1 μA after the proton beam irradiation at the same measurement conditions (an approximately 20% current increase). At the same time, the threshold voltage (V_{th}) shifted to the positive gate voltage direction (see also Fig. 3a). On the other hand, when the device was irradiated with a proton beam of a higher fluence of 10^{14} cm^{-2}, the device's current decreased, with ~3.0 μA at $V_{DS} = -30$ V and $V_G = -30$ V before proton irradiation decreasing to ~2.0 μA after proton irradiation at the same measurement

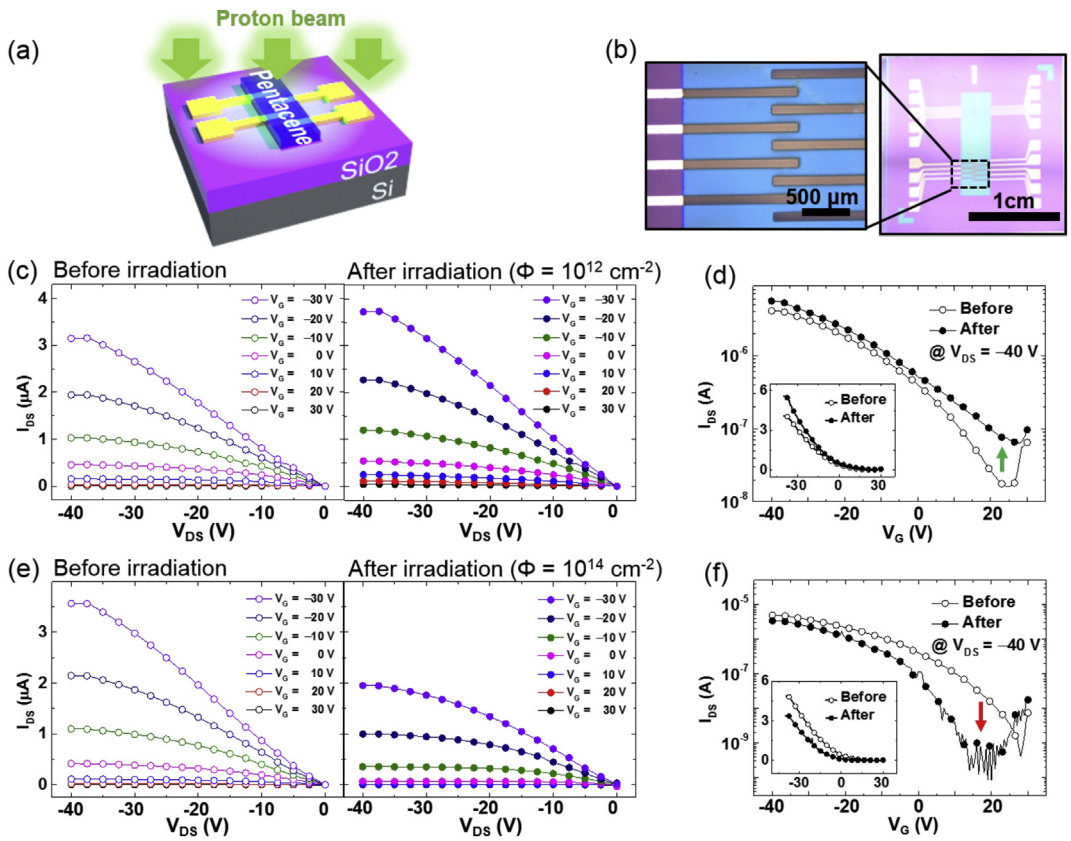

Fig. 1. (a) Schematic illustration of a pentacene OFET with proton beam irradiation. (b) Optical images of fabricated pentacene OFET devices. (c) Output characteristics and (d) transfer characteristics of pentacene OFET devices before and after proton beam irradiation with fluences of (c), (d) 10^{12} cm^{-2} and (e), (f) 10^{14} cm^{-2}. Insets in (d), (f) display the plots on the linear y-scale.

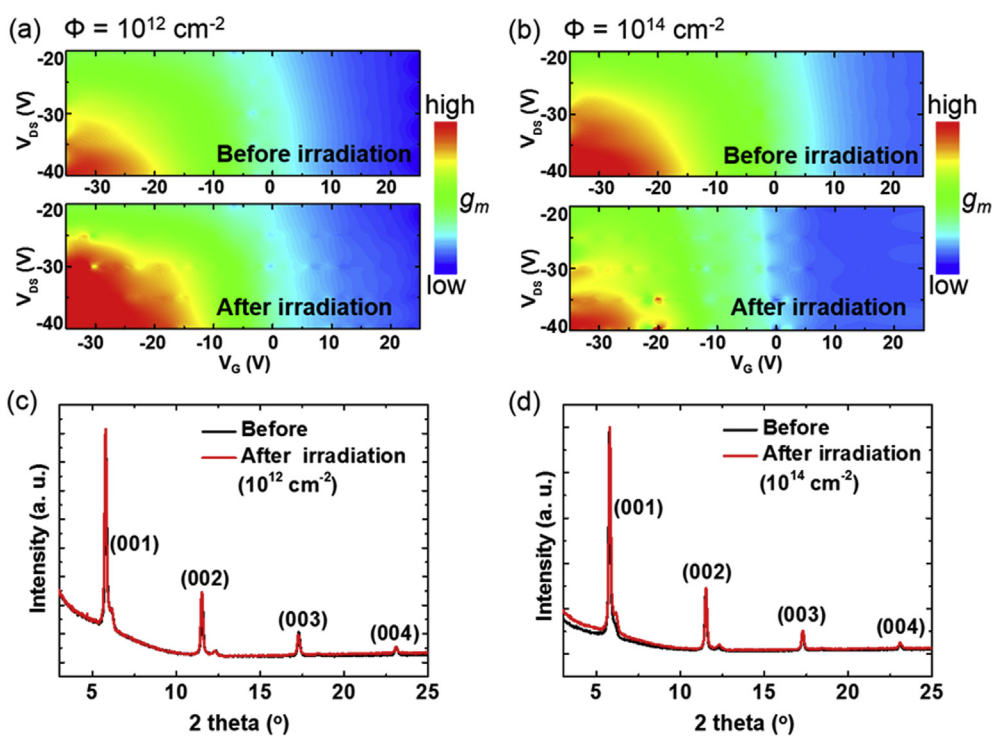

Fig. 2. Contour plots of transconductance of pentacene OFET devices before and after proton beam irradiation with fluences of (a) 10^{12} cm^{-2} and (b) 10^{14} cm^{-2}. XRD patterns of pentacene layers before and after proton beam irradiation with fluences of (c) 10^{12} cm^{-2} and (d) 10^{14} cm^{-2}.

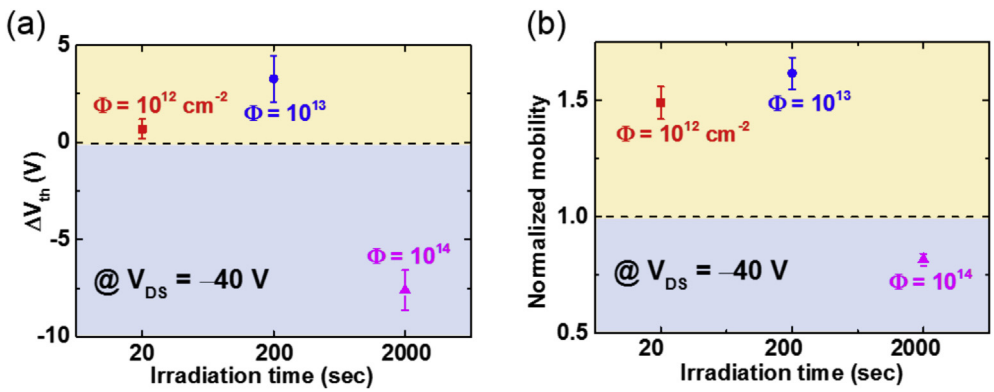

Fig. 3. Statistical data for (a) the change in the threshold voltage and (b) normalized mobility of pentacene OFET devices following proton beam irradiation with fluences of 10^{12}, 10^{13}, and 10^{14} cm^{-2}.

conditions (~33% current decrease). Correspondingly the threshold voltage shifted to the negative gate voltage direction (see Fig. 3a). For the case of proton beam irradiation with a fluence condition of 10^{13} cm^{-2}, corresponding to an irradiation time of 200 s, the electrical characteristics change of the device was similar to that of the low-fluence condition of 10^{12} cm^{-2} (see Fig. S2 of the Supplementary Data). For reference, the $|I_{DS}|^{0.5}$ versus V_G transfer characteristics data are provided in Fig. S4a–c of the Supplementary Data.

In accordance with the shift of threshold voltage, Fig. 2a and b show two-dimensional contour plots of transconductance ($g_m = I_{DS}/V_G$) which is an important parameter related to FET operation. Originally, the transconductance increased with increasing negative V_{DS} and V_G, regardless of the proton beam irradiation (see the upper figures of Fig. 2a and b before proton beam irradiation) Then, the transconductance increased after the low-fluence (10^{12} cm^{-2}) proton beam irradiation, whereas it decreased after the high-fluence (10^{14} cm^{-2}) proton beam irradiation at a given gate voltage condition (for example, see the transconductance before and after the proton beam irradiation at $V_G = -20$ V and $V_{DS} = -30$ V in Fig. 2a and b). In the case of the fluence condition of 10^{13} cm^{-2}, the transconductance followed a similar phenomenon to the case of the low-fluence condition of 10^{12} cm^{-2}, with the increasing transconductance after proton beam irradiation (see Fig. S3a of the Supplementary Data). Here, the transconductance changes after the proton beam irradiation are associated with the proton irradiation-induced charges in the semiconducting pentacene and in the dielectric SiO_2 layers [29], which will be explained later. Detailed device performance parameters such as threshold voltage, mobility, subthreshold swing, and ON-state I_{DS} are listed in Tables S1–S3 of the Supplementary Data.

To investigate whether the proton beams altered the pentacene active film directly or not, we examined and compared the pentacene layers before and after proton beam irradiation by using X-ray diffraction (XRD) and atomic force microscopy (AFM) measurements. Fig. 2c and d show XRD patterns obtained from pentacene layers before and after the proton beam of fluence conditions of 10^{12} cm^{-2} and 10^{14} cm^{-2}, respectively. The observed XRD peak positions of the pentacene films prior to proton beam irradiation coincided with data reported in the literature [30,31]. More importantly, we observed that there was no noticeable XRD peak change after the proton beam irradiation, which suggests that the structure of the pentacene layer did not change significantly after the proton beam irradiations. Similar XRD patterns were also observed for the 10^{13} cm^{-2} fluence beam condition (see Fig. S3b of the Supplementary Data). We also examined the pentacene layer's morphology with AFM before and after the proton beam irradiations, and could not observe any noticeable change in the surface morphology after the proton beam irradiations (data are not shown here). Furthermore, we calculated the energy-loss depth profiles of the irradiated protons using the Stopping and Range of Ions in Matter (SRIM 2008) software, which is a computer program that calculates the interactions of energetic particles with matter [32,33]. The SRIM simulation results are provided in Fig. S5 of the Supplementary Data. From the SRIM simulation results, we found that protons could penetrate ~700 μm into the top surface before stopping loosing most of their energy there. Because the structure of our pentacene OFET devices comprised stacks of pentacene/SiO_2/p++Si (60 nm/270 nm/500 μm), the majority of protons penetrated through the entire structure while transferring small amount of energy. Therefore, we can assume that the pentacene layer itself is not directly deteriorated by the proton beam and the observed changes in the electrical properties (Fig. 1c–f and Fig. 2a and b) would not be due to the transformation of pentacene layer. Rather, the changes are due to proton beam irradiation-induced charges created in the semiconducting pentacene and dielectric SiO_2 layers (the detailed mechanism of the proton beam irradiation effects on the devices are explained in Fig. 4).

Fig. 3a summarizes the statistical analysis of the shift of threshold voltage of the pentacene OFET devices after the proton beam irradiations of three fluence conditions of 10^{12} cm^{-2}, 10^{13} cm^{-2}, and 10^{14} cm^{-2}. As stated earlier, we used more than 5 devices for each irradiation condition and the error bars in the figures are the standard deviations from the individual measurements. As previously presented, the threshold voltage of the devices shifted to the positive gate voltage direction after irradiation with proton beams of fluence conditions of 10^{12} cm^{-2} or 10^{13} cm^{-2}, whereas it shifted to the negative gate voltage direction for the 10^{14} cm^{-2} fluence condition. The threshold voltage increased from −7.2 to −6.2 V and −9.6 to −6.4 V after proton beam irradiation for 10^{12} cm^{-2} and 10^{13} cm^{-2}, respectively. However, it decreased from −10.3 to −17.8 V after proton beam irradiation for 10^{14} cm^{-2}.

Fig. 3b shows the changes in the normalized mobility of the devices after the proton beam irradiations of the three fluence conditions. The normalized mobility value is the ratio of the field-effect mobility of the pentacene OFET devices after the proton beam irradiation to that of the devices before the irradiation. The field-effect mobility values of our pentacene OFETs before the proton irradiation were found to be ~1.0 cm^2/V s (See Tables S1–S3 of the Supplementary Data). When the devices were irradiated with 10^{12} cm^{-2} and 10^{13} cm^{-2} proton beams, the normalized mobility was observed to be larger than 1, that is, the mobility of

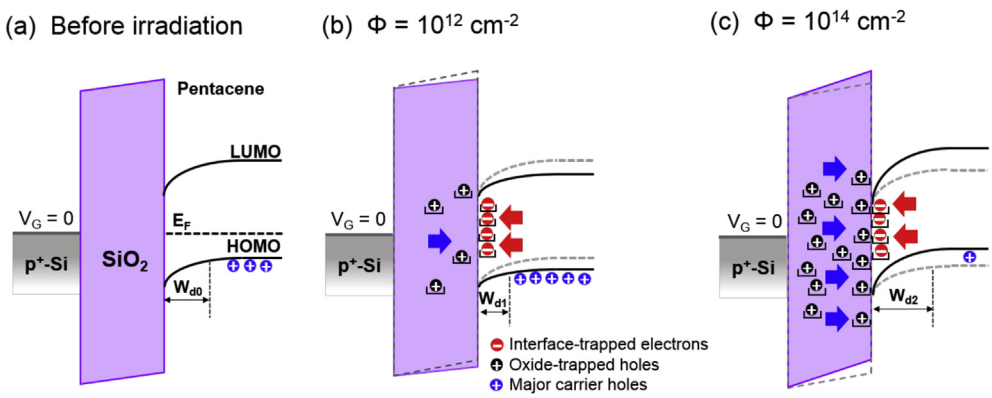

Fig. 4. Energy band diagrams of the pentacene OFET devices (a) before and (b), (c) after proton beam irradiation with fluences of (b) 10^{12} cm^{-2} and (c) 10^{14} cm^{-2}. Here, HOMO is the highest occupied molecular orbital and LUMO is the lowest unoccupied molecular orbital of pentacene.

the devices was enhanced. The field-effect mobility increased from 0.6 to 1.6 cm^2/V s and 0.8–1.3 cm^2/V s after proton beam irradiation for 10^{12} cm^{-2} and 10^{13} cm^{-2}, respectively. On the other hand, for the 10^{14} cm^{-2} fluence condition, the normalized mobility was less than 1, that is, the mobility of the devices was reduced after the proton beam irradiation. The field-effect mobility values decreased from 1.0 to 0.8 cm^2/V s after proton beam irradiation for 10^{14} cm^{-2}. These phenomena are associated with transconductance changes caused by the proton beam irradiation (Fig. 2a and b). The transconductance was enhanced after the devices were irradiated with 10^{12} cm^{-2} and 10^{13} cm^{-2} proton beams (Fig. 2a and Fig. S3a), so the mobility was also enhanced for these fluence conditions (Fig. 3b), whereas the transconductance was reduced after the devices were irradiated with a 10^{14} cm^{-2} proton beam (Fig. 2b), so the mobility was also reduced for this fluence condition (Fig. 3b). The observed transconductance and mobility changes after proton irradiation can be attributed to the modulation of the channel current and gate electric field in the FET configuration because ionizing irradiation with high energetic particles can generate irradiation-induced electron–hole pairs in pentacene and SiO_2 layers [34–36].

Now, we explain the experimental observations of the proton beam irradiation effects on the pentacene OFET devices. There are two aspects to consider here. First, when the FETs with semiconductor/oxide (SiO_2)/metal structure are irradiated by a high-energy proton beam, electron–hole pairs are generated in the semiconducting channel, dielectric oxide, and metallic layers [37]. Usually, electron–hole pairs generated in the metallic layer quickly move out away [38]. In contrast, only the irradiation-induced electrons inside the SiO_2 dielectric layer which has much higher mobility than irradiation-induced holes can be rapidly swept out of the bulk SiO_2 layer [39]. As a result, some of the irradiation-induced holes left can be trapped at localized sites in the bulk SiO_2 layer, leading to positive oxide-trapped charges in the SiO_2. As the beam irradiation time increases, some fraction of these irradiation-induced holes can migrate to the SiO_2/semiconductor interface, resulting in the formation of irradiation-induced trap states near the interface. The second aspect to consider on the proton beam irradiation effects is following. High energetic proton beam can generate electron–hole pairs in the semiconducting pentacene layer as well. In particular, the electrons induced by electron–hole pair generation inside the pentacene layer can be trapped at the hydroxyl groups of pentacene/SiO_2 interface [11,21]. Several studies about UV irradiation effects on pentacene/SiO_2 FETs showed such negative charge trapping phenomenon [21,41]. In the same manner, in our proton beam irradiation research, electrons induced by the electron–hole pair generation in the pentacene layer can be trapped at the pentacene/SiO_2 interface; we will call these as "interface-trapped electrons" from now on.

Fig. 4a–c show the energy band diagrams of p-type pentacene OFETs with a p++Si back-gated configuration before and after the proton beam irradiations. When a pentacene active layer is deposited on the SiO_2/Si substrates, there are interface states on the interface between the pentacene and SiO_2 layers [40]. These interface states can trap hole carriers of the p-type pentacene layer (not depicted in Fig. 4), creating a slightly depleted region (W_{d0} in Fig. 4a) in the pentacene channel near the interface. In the case of low-fluence proton irradiation condition (10^{12} cm^{-2}) on the pentacene OFET (Fig. 4b), the effect of irradiation-induced positive oxide-trapped charges in the SiO_2 dielectric layer is relatively weaker than the effect of interface-trapped electrons induced by electron–hole pair generation in the pentacene layer. Specifically, these interface-trapped electrons at the pentacene/SiO_2 interface will result in hole accumulation in the channel and a downward band-bending of highest occupied molecular orbital (HOMO) and lowest unoccupied molecular orbital (LUMO) levels, as depicted in Fig. 4b. In this figure, the dashed and solid lines mean the HOMO-LUMO levels before and after the proton-beam irradiation, respectively. This means that the electric field effect by the interface-trapped electrons (indicated with the red (in web version) arrows in Fig. 4b) overwhelms that of the irradiation-induced positive oxide-trapped charges inside the SiO_2 layer (indicated with the blue (in web version) arrow in Fig. 4b). In other words, these interface-trapped electrons at the pentacene/SiO_2 interface act like a negative gate voltage, resulting in the decrease of the surface depletion region (W_{d1} in Fig. 4b). As a result, the electric current, transconductance, and field effect mobility increase, and the threshold voltage shifts to the positive gate voltage direction.

In contrast, for the case of the high-fluence proton irradiation condition (10^{14} cm^{-2}), as the irradiation time increases, the amount of the irradiation-induced trapped positive charges originated from the SiO_2 dielectric layer increase. A large amount of trapped holes mainly exert an electrostatically repulsive force upon hole carriers in the pentacene channel over the effect of interface-trapped electrons induced by the electron–hole pair generation in the pentacene layer (see the increased number of blue arrows in Fig. 4c). This repulsive force can push the holes away from the interface, resulting in a larger surface depletion region (W_{d2} in Fig. 4c) moving HOMO and LUMO levels upward (also in this figure, the dashed and solid lines mean the HOMO-LUMO levels before and after the proton-beam irradiation, respectively). In particular, the increase of the surface depletion region can reduce the effective gate electric field. As a result, the electric current,

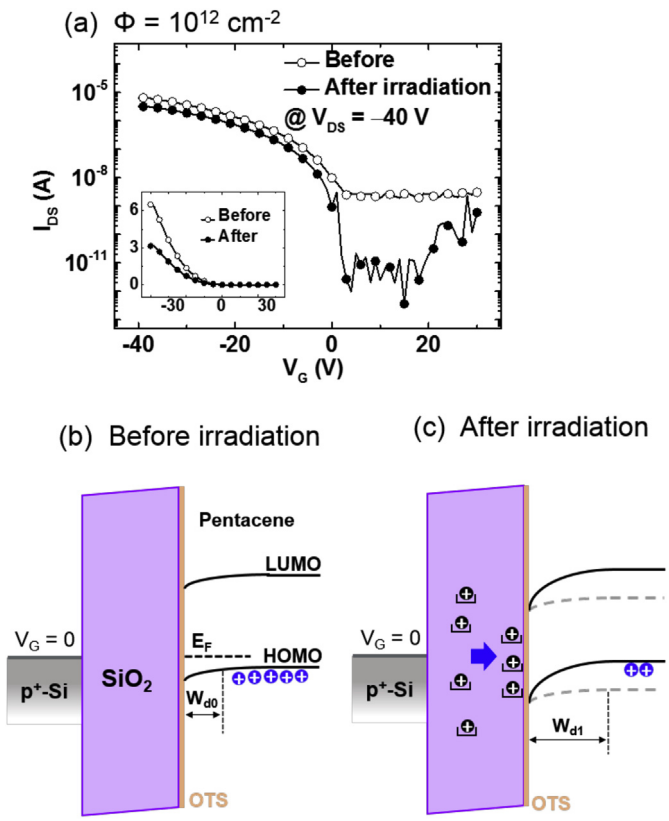

Fig. 5. (a) Transfer characteristics of OTS SAM-treated pentacene OFET devices before and after proton beam irradiation with a fluence of 10^{12} cm^{-2}. Energy band diagram of the devices (b) before and (c) after proton beam irradiation.

transconductance, and field effect mobility decrease, and the threshold voltage shifts to the negative voltage direction.

To further support our interpretation of the proton beam effects on the pentacene OFET devices, we fabricated another type of pentacene OFET device structure with a self-assembled monolayer (SAM) of octadecyltrichlorosilane (OTS) which is well-known for suppressing the interface trap states was coated on the surface of the SiO_2 dielectric layer. The detailed fabrication process of this type of device is explained in the Experimental Section and in the Supplementary Data (Fig. S6a). Fig. 5a shows the transfer characteristics (I_{DS}–V_G) measured at a fixed V_{DS} of −40 V before and after low-fluence (10^{12} cm^{-2}) proton beam irradiation. Unlike for the previously discussed devices (Fig. 1c and d), the current did not increase, but rather slightly decreased. The OTS layer is known for suppressing the number of interface states at the pentacene/SiO_2 interface [42,43]. Therefore, after the low-fluence proton beam irradiation, relatively smaller number of electrons induced by electron–hole pair generated in the pentacene layer can be trapped at the interface of the pentacene/SiO_2 layers. However, the irradiation-induced positive charges in the SiO_2 layer allow the major carrier holes to be depleted in the pentacene layer with the OTS SAM treatment, resulting in a current decrease after the low-fluence proton beam irradiation. This is schematically explained in the energy band diagrams in Fig. 5b and c. The dominant effect of the irradiation-induced positive charges inside the SiO_2 dielectric layer results in the increase of the surface depletion region (W_{d1} in Fig. 5c).

4. Conclusions

In summary, we studied the effect of proton beam irradiation on pentacene OFET devices. The devices exhibited increases in the current, transconductance, and mobility with a shift of the threshold voltage to the positive gate voltage direction after the devices were irradiated by proton beams with low fluence, whereas the devices exhibited decreases in the current, transconductance, and mobility with a shift of the threshold voltage to the negative gate voltage direction after the devices were irradiated by proton beams with high fluence. These phenomena can be attributed to the interplay between the proton irradiation-induced trapped charges at the pentacene/SiO_2 interface and in the SiO_2 layer. Our interpretation was supported by investigating the proton irradiation effect on pentacene OFET devices having suppressed interface states by treatment with an octadecyltrichlorosilane self-assembled monolayer on the SiO_2 surface. Our study enhances the understanding of the proton irradiation effect on organic electronic devices and may also provide a useful way to create property-tailored organic devices by proton beam irradiation.

Acknowledgments

The authors appreciate the financial support of the National Creative Research Laboratory program (Grant No. 2012026372) through the National Research Foundation of Korea (NRF) funded by the Korean Ministry of Science, ICT & Future Planning. We are especially thankful for the beam time grants from the proton beam facilities of the Korea Institute of Radiological and Medical Sciences.

W.-K. H acknowledges the financial support from the Basic Science Research Program through the NRF (Grant No. NRF-2013-R1A1A2009884), funded by the Ministry of Education

Appendix A. Supplementary data

Supplementary data related to this article can be found at http://dx.doi.org/10.1016/j.orgel.2015.09.029.

References

[1] H. Klauk, Organic Electronics II: More Materials and Applications, Wiley-VCH, Weinheim, Germany, 2012.
[2] Z. Bao, J. Locklin, Organic Field-effect Transistors, CRC Press, Boca Raton, FL, 2007.
[3] W.S. Wong, M.L. Chabinyc, T.N. Ng, A. Salleo, Flexible Electronics: Materials and Applications, Springer, NY, 2009.
[4] M. Iwamoto, Y.-S. Kwon, T. Lee, Nanoscale Interface for Organic Electronics, World Scientific, Singapore; Hackensack, NJ, 2011.
[5] C.D. Dimitrakopoulos, P.R.L. Malenfant, Adv. Mater. 14 (2002) 99.
[6] V. Subramanian, P.C. Chang, J.B. Lee, S.E. Molesa, S.K. Volkman, IEEE Trans. Compon. Packag. Technol. 28 (2005) 742.
[7] A. Dodabalapur, Mater. Today 9 (2006) 24.
[8] G.H. Gelinck, H.E.A. Huitema, E. van Veenendaal, E. Cantatore, L. Schrijnemakers, J.B.P.H. van der Putten, T.C.T. Geuns, M. Beenhakkers, J.B. Giesbers, B.H. Huisman, E.J. Meijer, E.M. Benito, F.J. Touwslager, A.W. Marsman, B.J.E. van Rens, D.M. de Leeuw, Nat. Mater. 3 (2004) 106.
[9] S. Ju, J.F. Li, J. Liu, P.C. Chen, Y.G. Ha, F. Ishikawa, H. Chang, C.W. Zhou, A. Facchetti, D.B. Janes, T.J. Marks, Nano Lett. 8 (2008) 997.
[10] S. Lee, G. Jo, S.J. Kang, G. Wang, M. Choe, W. Park, D.Y. Kim, Y.H. Kahng, T. Lee, Adv. Mater. 23 (2011) 100.
[11] L.–L. Chua, J. Zaumseil, J.–F. Chang, E.C.W. Ou, P.K.H. Ho, H. Sirringhaus, R.H. Friend, Nature 434 (2005) 194.
[12] D. Braga, G. Horowitz, Adv. Mater. 21 (2009) 1473.
[13] J. Lee, K. Kim, J.H. Kim, S. Im, D.Y. Jung, Appl. Phys. Lett. 82 (2003) 4169.
[14] J. Veres, S. Ogier, G. Lloyd, D. de Leeuw, Chem. Mater. 16 (2004) 4543.
[15] O.D. Jurchescu, M. Popinciuc, B.J. van Wees, T.T.M. Palstra, Adv. Mater. 19 (2007) 688.
[16] J. Takeya, M. Yamagishi, Y. Tominari, R. Hirahara, Y. Nakazawa, T. Nishikawa, T. Kawase, T. Shimoda, S. Ogawa, Appl. Phys. Lett. 90 (2007) 102120.
[17] S.J. Kang, G.H. Lee, Y.J. Yu, Y. Zhao, B. Kim, K. Watanabe, T. Taniguchi, J. Hone, P. Kim, C. Nuckolls, Adv. Funct. Mater. 32 (2014) 5157.
[18] S.A. DiBenedetto, A. Facchetti, M.A. Ratner, T.J. Marks, Adv. Mater. 21 (2009) 1407.
[19] H. Klauk, M. Halik, U. Zschieschang, G. Schmid, W. Radlik, W. Weber, J. Appl. Phys. 92 (2002) 5259.
[20] Y. Jang, J.H. Cho, D.H. Kim, Y.D. Park, M. Hwang, K. Cho, Appl. Phys. Lett. 90 (2007) 132104.
[21] Y.Y. Noh, J. Ghim, S.J. Kang, K.J. Baeg, D.Y. Kim, K. Yase, J. Appl. Phys. 100

(2006) 094501.
[22] H. Yano, T. Hirao, T.Z. Duan, Y. Takayanagi, H. Ohuchi, H. Ueki, T. Ohshima, Adv. Mater. Res. 306 (2011) 185.
[23] G. Jo, W.-K. Hong, J.I. Sohn, M. Jo, J. Shin, M.E. Welland, H. Hwang, K.E. Geckeler, T. Lee, Adv. Mater. 21 (2009) 2156.
[24] S. Ju, K. Lee, D.B. Janes, R.C. Dwivedi, H. Baffour-Awuah, R. Wilkins, M.-H. Yoon, A. Facchetti, T.J. Mark, Appl. Phys. Lett. 89 (2006) 073510.
[25] T.-Y. Kim, K. Cho, W. Park, J. Park, Y. Song, S. Hong, W.-K. Hong, T. Lee, ACS Nano 8 (2014) 2774.
[26] T.R. Oldham, Ionizing Radiation Effects in MOS Oxides, vol. 3, World Scientific, 1999.
[27] T.P. Ma, P.V. Dressendorfer, Ionizing Radiation Effects in MOS Devices and Circuits, Wiley, NY, 1989.
[28] H.N. Raval, S.P. Tiwari, R.R. Navan, V.R. Rao, Appl. Phys. Lett. 94 (2009) 123304.
[29] W.-K. Hong, G. Jo, J.I. Sohn, W. Park, M. Choe, G. Wang, Y.H. Kahng, M.E. Welland, T. Lee, ACS Nano 4 (2010) 811.
[30] D. Knipp, R.A. Street, A. Volkel, J. Ho, J. Appl. Phys. 93 (2003) 347.
[31] H.-L. Cheng, Y.-S. Mai, W.-Y. Chou, L.-R. Chang, Appl. Phys. Lett. 90 (2007) 171926.
[32] J.F. Ziegler, J.P. Biersack, The Stopping and Range of Ions in Matter, Springer, 1985.
[33] J.F. Ziegler, M.D. Ziegler, J.P. Biersack, Nucl. Instrum. Methods Phys. Res. Sect. B 268 (2010) 1818.
[34] T.R. Oldham, F. McLean, IEEE Trans. Nucl. Sci. 50 (2003) 483.
[35] S.M. Sze, K.K. Ng, Physics of Semiconductor Devices, third ed., Wiley-Interscience, 2007. Chapter 4.
[36] J.R. Schwank, M.R. Shaneyfelt, D.M. Fleetwood, J.A. Felix, P.E. Dodd, P. Paillet, V. Ferlet-Cavrois, IEEE Trans. Nucl. Sci. 55 (2008) 1833.
[37] R.P. Feynman, R.B. Leighton, M. Sands, Lectures on Physics, vol. 3, Addison-Wesley, Reading, MA, 1966. Chapter 14.
[38] B.I. Kharisov, O.V. Kharissova, U.O. Mendez, Radiation Synthesis of Materials and Compounds, CRC Press, 2013. Chapter 8.
[39] R. Hughes, Phys. Rev. Lett. 30 (1973) 1333.
[40] L.W. Chen, R. Ludeke, X.D. Cui, A.G. Schrott, C.R. Kagan, L.E. Brus, J. Phys. Chem. B 109 (2005) 1834.
[41] J.-M. Choi, D.K. Hwang, J.M. Hwang, J.H. Kim, S. Im, Appl. Phys. Lett 90 (2007) 113515.
[42] J.E. McDermott, M. McDowell, I.G. Hill, J. Hwang, A. Kahn, S.L. Bernasek, J. Schwartz, J. Phys. Chem. A 111 (2007) 12333.
[43] X.H. Zhang, S.P. Tiwari, B. Kippelen, Org. Electron. 10 (2009) 1133.